Synthesis and characterization of organically modified attapulgite/polyurethane nanocomposites

Chia-Hao Wang [1,*], Maria L. Auad [2], Norma E. Marcovich[3] and Steven Nutt[1]

1. Gill Foundation Composites Center, Materials Science Department, University of Southern California, Los Angeles, CA 90089-0241
2. Polymer and Fiber Engineering Department, Auburn University, Auburn, AL 36849-5327
3. Institute of Materials Science and Technology (INTEMA), University of Mar del Plata, 7600 Mar del Plata, Argentina

Abstract: Polyurethane (PU) nanocomposites filled with attapulgite (ATT) nanorods were synthesized and characterized with thermal analysis, dynamic mechanical analysis (DMA), and mechanical testing. The formulations were based on 4,4′-methylene bis(phenyl isocyanate) (MDI), polytetrahydrofuran, 1,4-butanediol, and inorganic ATT premodified with MDI. The original and premodified ATT (ATT–OH and ATT–MDI) nanorods were characterized with thermogravimetric analysis (TGA) and Fourier transform infrared (FTIR) spectroscopy. The analysis revealed that 17 wt % MDI was grafted/adsorbed onto the surface of ATT as a result of the modification. Pristine PU and ATT–MDI/PU nanocomposites were characterized with scanning electron microscopy, differential scanning calorimetry, and TGA. The mechanical tests and DMA showed an increase in the storage modulus and Young's modulus with increasing ATT–MDI content. The crystallinity of the hard and soft segments and thermal stability showed enhancements over those of the neat resin.

Key words: clay; fillers; nanocomposites; polyurethanes; reinforcement

1. Introduction

Segmented polyurethane (PU) elastomer is an important engineering polymer with widespread commercial applications. Among its attributes are high abrasion resistance, shock absorption,

Please cite this article as: C-H Wang, M.L. Auad, N.E. Marcovich, and S. Nutt. **Synthesis and characterization of organically modified attapulgite/polyurethane nanocomposites**, J App Polymer Sci 109 [4] (2008) 2562-2570. DOI:http://dx.doi.org/doi:10.1002/app.28254

flexibility, elasticity, and resistance to chemicals. These properties originate primarily from the special tendency of PU to form discrete regions of microdomains. The linear chain structure of PU can be expressed in the form of (A–B)n, where the hard segment A is composed of a low-molecular-weight diol or diamine (chain extender) with diisocyanate and the soft segment B is composed of a high-molecular-weight polyester or polyether polyol. Because of the different chemical structures of the hard and soft segments, repulsive interactions and thermodynamic incompatibility lead to phase separation [1] and the formation of hard- and soft-segment domains. Moreover, the hard segments form microdomains by intermolecular hydrogen bonding in the PU network [2].

Two approaches can be used to enhance the mechanical properties and thermal stability of PUs. The first is to change the molecular structure of the PU. Because the properties of PU polymers depend on the molar ratio of the diisocyanate, polyol, and chain extender, PU can be readily engineered to achieve a wide range of specific properties [3]. In the second approach, inorganic fillers can be introduced into the PU matrix.

Attapulgite (ATT) is a hydrated magnesium aluminum silicate with the chemical formula $Si_8O_{20}A_{l2}$ $Mg_2(OH)_2(OH_2)_4(4H_2O)$ [4]. Although ATT features ribbons of a 2 : 1 phyllosilicate structure, it differs from other layered silicates in that it lacks continuous octahedral sheets. Each ribbon is linked to the next by the inversion of SiO_4 tetrahedra along a set of Si-O-Si bonds that extend parallel to the x axis, forming rectangular channels that contain zeolitic water [5]. However, the Si-O-Si bonds are weak and are broken easily by shear stress to form fiber crystals [5]. The average external and internal surface areas have been estimated to be 300 and 600 m2/g, respectively.5 Because of the unique morphology and structure, ATT has been used for various commercial applications, such as adsorbents, catalysts, rheological agents, and fillers [5–9].

Please cite this article as: C-H Wang, M.L. Auad, N.E. Marcovich, and S. Nutt. **Synthesis and characterization of organically modified attapulgite/polyurethane nanocomposites**, J App Polymer Sci 109 [4] (2008) 2562-2570. DOI:http://dx.doi.org/doi:10.1002/app.28254

Despite the relatively low cost and availability of such nanosilicates, ATT did not draw much attention in polymer research until organic–inorganic nanocomposites based on layered silicates were first introduced by the Toyota Research Center (combining nylon and montmorillonite) [10–12]. Since then, small amounts of ATT have been used to improve the mechanical properties and thermal stability of polymeric matrices through the exploitation of the large specific surface area and unusual rodlike morphology of this type of nanoclay [13–17]. On the other hand, recent studies have reported that anisotropic carbon nanotubes (CNTs) are effective reinforcing fibers for composites because of their high aspect ratio, mechanical strength, conductivity, and thermal stability [18–22] For example, the addition of CNTs to PU reportedly increased the elastic modulus by 38 and 60% with 2 wt % concentrations of multiwalled and single-walled CNTs, respectively [23]. However, a major challenge for such composites lies in the processing, particularly in achieving a uniform dispersion of the CNTs in the polymer matrix. The substitution of rigid, rodlike silicates such as ATT in place of CNTs may be an alternative for enhancing polymer properties without sacrificing the nanoscale dispersion.

The interfacial adhesion between the dispersed and continuous phases, as well as the dispersion of the reinforcing phase, directly affects the mechanical properties of composites. For inorganic fillers, surface modification is the most common and efficient way of obtaining strong interfacial adhesion. The aim of this work was to determine the effect of the ATT surface treatment on the composite mechanical behavior and thermal stability. ATT nanorods were treated with chemical agents to generate an organophilic character on the hydrophilic silicate surface to improve the compatibility with the PU matrix. The chemical modifications were confirmed by thermogravimetric analysis (TGA) and FTIR studies. Subsequently, nanorods of ATT and 4,4′-methylene bis(phenyl isocyanate) (MDI) were incorporated into the PU matrix by in situ polymerization, and ATT–MDI/PU

nanocomposites were produced. The physical, mechanical, and thermal properties of ATT–MDI/PU nanocomposites with different ATT loadings and chemical affinities were investigated.

2. Experimental

2.1 Materials

ATT (Engelhard Co., Iselin, NJ) was subjected to purification with the polymeric dispersant sodium polyacrylate (molecular mass ~ 4000–5000) [24]. After dehydration, 1,4-butanediol (BDO; Avocado Research Chemicals, Ltd., Morecambe, UK) and polytetrahydrofuran (PTHF; BASF; molecular weight = 2900 Florham Park, NJ), which are a hydroxyl-terminated monomer and oligomer, respectively, were used for the preparation of PU networks. The isocyanate MDI (98%; Sigma-Aldrich, St. Louis, MO) was purified by the filtration of a molten MDI liquid at 70°C. Dimethylformamide (DMF; Sigma-Aldrich) was used as a media solvent in the polymerization reaction.

2.2 Preparation of ATT-OH and ATT-MDI

Figure 1 shows the modification and chemical structure of the ATT nanorods. The polymeric dispersant was removed from ATT surfaces through heating at 500°C for 1 h. Next, ATT nanorods were treated with 5*M* hydrochloric acid at 80°C for 1 h to produce hydroxyl groups on the nanorod surfaces and remove residual sodium ions and impurities. After exhaustive washing with deionized water and acetone, the ATT–OH nanorods were dried at 80°C *in vacuo* for 24 h. Subsequently, the dried ATT–OH was ground into a powder and dispersed in 600 mL of acetone by an ultrasonic treatment. To graft isocyanate molecules onto the nanorod surface, excess (8–10 g) dehydrated MDI

was added to 10 g of ATT–OH, [25] and the mixture was refluxed at 80°C for 1 h. After grafting, the ATT–MDI nanorods were washed three to four times with acetone, centrifuged at 4000 rpm to remove ungrafted MDI, and finally dried at 80°C *in vacuo* for 24 h. The dried cake was ground and screened through a 325-mesh sieve to obtain the organically modified ATT (ATT–MDI). TGA and Fourier transform infrared (FTIR) spectroscopy were used to determine the amount of MDI grafted onto the surface of ATT and to identify the chemical bonds.

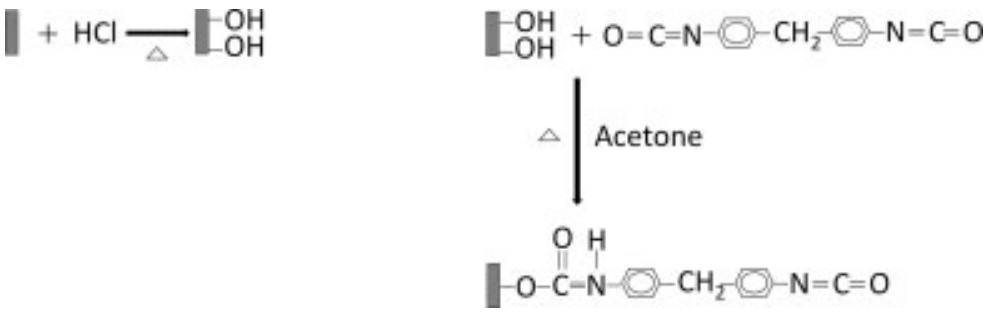

Figure 1: *Modification and chemical structure of the ATT nanorods.*

2.3Synthesis of the PU elastomers and ATT/PU composites

PU elastomer was synthesized with a 4 : 1 : 2.64 molar ratio of MDI/PTHF/BDO with excess diisocyanate to produce partially crosslinked networks [26]. First, the oligomeric polyol (PTHF) was dissolved in DMF and reacted with MDI at 80°C for 30 min to obtain a prepolymer. Second, the chain extender (BDO) was added to build up the PU network and allowed to react at 80°C for another 2 additional min. Finally, the mixture was poured into a Teflon mold and cured at 80°C for 24 h to obtain the PU elastomer.

Three types of ATT/PU composites were also prepared with identical molar ratios, as shown in Table I. To prepare ATT–MDI/PU nanocomposites, different amounts of ATT–MDI nanorods (0.5, 2.5, 5, and 10 wt %) were directly blended with PTHF, which was dissolved in the DMF

solvent, with a high-speed dual-axis mixer (HM-500, Keyence, Woodcliff Lake, NJ) for 30 min to form OH-terminated urethane oligomers. Next, excess MDI was added to the mixture, and the prepolymer was formed at 80°C in vacuo for 30 min. Subsequently, the chain extender BDO was added to the prepolymer with vigorous stirring for 2 min to complete the reaction. Finally, the viscous polymer was poured into a Teflon mold and cured at 80°C for 24 h to form ATT–MDI/PU nanocomposites. Figure 2 illustrates the steps in the synthesis route and the associated chemical structures. In addition, the acid-treated ATT (ATT–OH) and original ATT were also incorporated into the PU polymer for comparison with the 2.5 wt % ATT–MDI nanocomposite. These composites were prepared by the same procedure used for the former polymerization reaction.

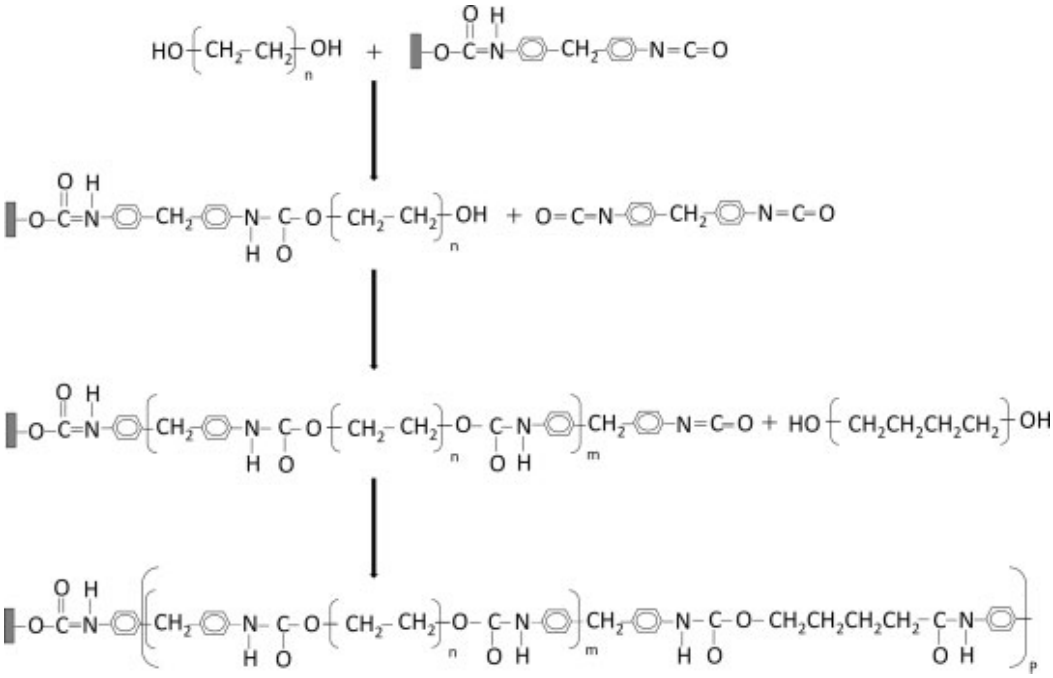

Figure 2: *Synthesis and chemical structure of the ATT–MDI/PU nanocomposite.*

Please cite this article as: C-H Wang, M.L. Auad, N.E. Marcovich, and S. Nutt. **Synthesis and characterization of organically modified attapulgite/polyurethane nanocomposites**, J App Polymer Sci 109 [4] (2008) 2562-2570. DOI:http://dx.doi.org/doi:10.1002/app.28254

Table 1: *Neat PU and ATT/PU Nanocomposite.*

Sample	PTHF (mol)	MDI (mol)	BD (mol)	Clay content (wt %)
Neat PU	1	4	2.64	0
0.5 wt % ATT–MDI/PU	1	4	2.64	0.5
2.5 wt % ATT–MDI/PU	1	4	2.64	2.5
5 wt % ATT–MDI/PU	1	4	2.64	5
10 wt % ATT–MDI/PU	1	4	2.64	10
2.5 wt % ATT–OH/PU	1	4	2.64	2.5
2.5 wt % ATT/PU	1	4	2.64	2.5

2.4Characterization

The ATT morphology was observed with transmission electron microscopy (TEM; model 420, Philips, Eindhoven, Netherlands) at 120 kV. TGA (TGA 2050, TA Instruments, New Castle, DE) was performed to determine the amount of diisocyanate grafted onto the surface of ATT nanorods and to identify the thermal decomposition temperatures of ATT–MDI/PU nanocomposites. In both cases, samples were heated to 800°C at 10°C/min under a nitrogen flow.

The grafting of functional groups was confirmed by FTIR spectroscopy in the transmission mode (model 4700, Nicolet, Waltham, MA).

The transition temperatures of soft and hard segments in ATT/PU composites were measured with differential scanning calorimetry (DSC; DSC 2920, TA Instruments). Measurements were performed with two scans to avoid signal noise and to erase the thermal history. In the first scan, the sample was heated to 250° (at 10°/min) and then cooled to −65°C. In the second scan, the sample was heated to 300° at a heating rate of 10°/min. The second scan was used to record transition temperatures.

The morphology of ATT–MDI/PU nanocomposite fracture surfaces was investigated with scanning electron microscopy (SEM; model 360, Cambridge; 15 kV, Cambridge, UK). The samples were gold-coated before SEM examination. The dispersion of the ATT–MDI nanorods in the PU matrix was observed with TEM (model 420, Philips) at 120 kV. Samples were sectioned with a microtome.

The storage modulus (G′) was assessed with dynamic mechanical analysis (DMA; DMA 2980, TA Instruments). Tests were conducted with the temperature scan mode from room temperature to 200°C at a 10°/min heating rate. The frequency of the forced oscillations was set to 1 Hz, and the applied deformation was 0.05%.

The tensile strength and modulus were measured with a universal testing machine (model 8531, Instron, Norwood, MA). Tests were performed on dog-bone-shaped specimens with a crosshead speed of 10 mm/min at room temperature in accordance with ASTM D 638-94b.

3. Results and Discussion

3.1 Characterization of ATT

The fibrous morphology of unmodified ATT was revealed by TEM (Fig. 3). In the pristine condition, the fibers were rod-shaped and formed a randomly oriented, densely packed network. The ATT nanorods were approximately 15–20 nm in diameter and several micrometers long. The high aspect ratio (length-to-diameter) resulted in a high specific surface area to interact with the continuous polymeric matrix. Thus, strong interactions between ATT particles and PU were expected.

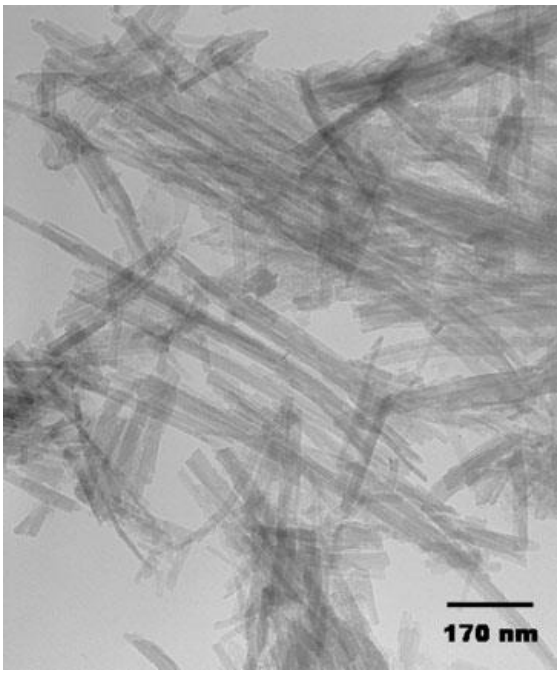

Figure 3: *TEM image of the original ATT.*

Figure 4 shows the thermogravimetric curves for pristine ATT and modified ATT (ATT–OH and ATT–MDI). The mass loss of the original ATT below 120°C was attributed to the evaporation of a small amount of adsorbed moisture. Discounting the mass loss of the original ATT, we found that the mass fraction of organic groups eliminated at 600°C was approximately 5.5 wt % for ATT–OH and 17 wt % for ATT–MDI. These values indicate that the two-step surface modification process led to a significant mass fraction of organic groups bonded to ATT. Additional insight could be gained by the comparison of the experimental mass fractions with those expected from a complete reaction of OH with MDI groups. Approximately 5.5 g of OH attached to 94.5 g of the original ATT could incorporate 80.9 g of MDI, leading to a theoretical organic mass fraction of 86% at full conversion, which is much greater than the measured value of 17%. The difference was attributed to the consumption of NCO groups by moisture (possibly residual zeolitic water) to form urea.

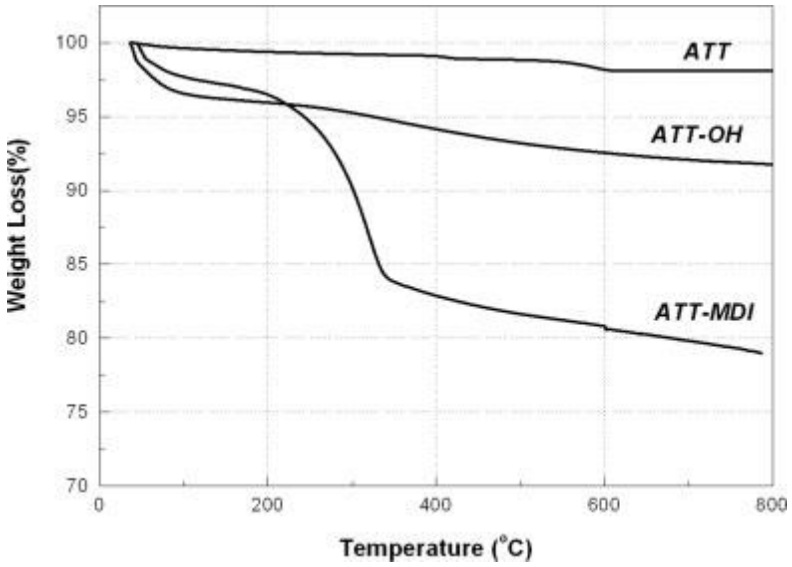

Figure 4: *TGA curves for the ATT nanorods before and after modification.*

In Figure 5(a), the spectrum for the original ATT reveals characteristic absorption bands at 3632 (from O—H stretching) and 1044 cm^{-1} (for Si—O in-plane stretching) [27]. The acid treatment of ATT (ATT–OH) and the grafting of functional groups on ATT (ATT–MDI) were also verified by FTIR, as shown in Figure 5(b,c). In the high wave-number region, a broad band at 3600–3200 cm^{-1} was attributed to adsorbed water molecules, and the band increased after the acid attack. (The peak at 3600–3550 cm^{-1} was attributed to OH stretching in hydrogen-bonded hydroxyls, and the peak at 3400–3200 cm^{-1} was attributed to OH stretching in free or weakly hydrogen-bonded hydroxyls). The band that appeared at 1625 cm^{-1}in the original ATT and shifted to 1600 cm^{-1} with increased intensity in ATT–OH was caused by the bending vibration mode of adsorbed water [28]. In addition, after the acid treatment, the absorption band at 880 cm^{-1} disappeared, and the characteristic band that appeared at 960–920 $cm^{-1}$was attributed to the Si—O—H angle deformation vibration for acid-treated ATT [29].

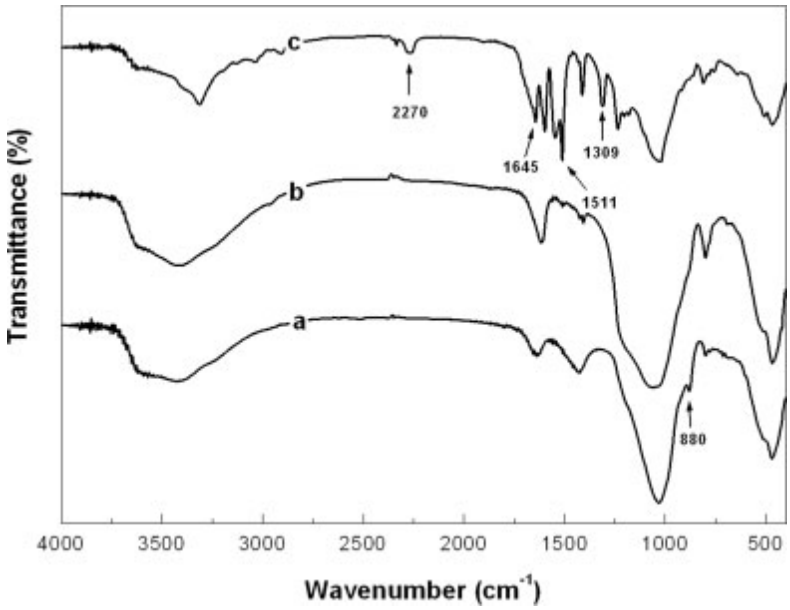

Figure 5: *FTIR spectra for the (a) original ATT, (b) ATT–OH, and (c) ATT–MDI.*

The two main regions of interest in the ATT–MDI spectrum are NH absorption and C═O stretching. The NH absorption peak at 3320 cm^{-1} can be attributed to hydrogen-bonded NH groups of urethane linkages [30]. The small shoulder, seen at 3420 cm^{-1}, is characteristic of the stretching of free NH groups. Moreover, the broad band arising from adsorbed water in the high wave-number region is absent in this spectrum, and this indicates that the hydrophilic character of ATT–MDI strongly decreased. On the other hand, peaks in the 1735–1690-cm^{-1} region, expected from free and hydrogen-bonded urethane carbonyl, are almost imperceptible at this scale. However, the absorbance due to the stretching of NCO groups at 2270 cm^{-1} [30] can be clearly discerned. The amide bands at 1645, 1511, and 1309 cm^{-1}, assigned to CO (amide I), NH (amide II), and CNH (amide III), respectively, which are consistent with polyurea formation, [30–32] can also be clearly observed. These results indicate that some of the MDI molecules were grafted onto the ATT surface through chemical bonding (according to Fig. 1), although the remainder may have been consumed in the formation of urea, which should be strongly adsorbed onto the ATT surface.

3.2 ATT/PU composites

3.2.1 DSC measurements

The DSC results for neat PU and ATT/PU composites are summarized in Table II. The data show evidence of profound differences in structure resulting from the addition of ATT to the PU networks. Because the structure of PU includes hard and soft segments, two melting temperatures were expected. However, the DSC curve revealed only one peak, and this was associated with the melting temperature of the soft segment. The peak associated with the melting temperature of the hard segment was absent from the DSC curve [33–35]. The absence was attributed to the inactive movement of the hard segment, which had a small heat capacity change, [36] and to the widely dispersed hard-segment microdomains within the PU matrix [37].

Table 2: *Thermal Properties of Neat PU and the ATT/PU Composites*

Sample	$T_{m,ss}$ **(°C)**[a]	**Δ*H* (J/g)**
Neat PU	21.6	37.8
0.5 wt % ATT–MDI/PU	25.5	43.2
2.5 wt % ATT–MDI/PU	25.3	44.3
5 wt % ATT–MDI/PU	27.9	46.5
10 wt % ATT–MDI/PU	25.0	38.5
2.5 wt % ATT–OH/PU	23.2	43.6
2.5 wt % ATT/PU	25.5	40.2

a Melting temperature of the soft segment. ΔH, enthalpy change.

The melting points in the region between 21.6 and 27.9°C are characteristic of ordered soft-segment structures and indicate that PTHF crystallized in both neat PU and ATT/PU composites. For these soft segments, the enthalpy change of ATT–MDI/PU nanocomposites increased from 43.2 to 46.5 J/g with increasing ATT–MDI content. This increase in the soft-segment melting temperature and

Please cite this article as: C-H Wang, M.L. Auad, N.E. Marcovich, and S. Nutt. **Synthesis and characterization of organically modified attapulgite/polyurethane nanocomposites**, J App Polymer Sci 109 [4] (2008) 2562-2570. DOI:http://dx.doi.org/doi:10.1002/app.28254

enthalpy change can be attributed to the effects produced by the rigid nanofillers in the soft-segment domains, which acted as nucleation seeds, increasing the degree of crystallinity of the PU networks [38]. Moreover, these values increased with ATT–MDI concentrations up to 5% and then decreased for the 10% sample. This behavior was attributed to the reduction in the effective surface area caused by particle agglomeration at high ATT–MDI contents. Similarly, for both ATT–OH/PU and ATT/PU composites, the soft-segment melting temperature and enthalpy change increased with respect to neat PU, indicating that the crystalline nanorods of the ATT–OH and original ATT also acted as seeds to nucleate and enhance the crystallinity of the PU matrix. On the other hand, when the ATT concentration was held constant at 2.5%, the ΔH (enthalpy change) values differed with the ATT treatment, indicating that the compatibility of the filler with the matrix also played a significant role in the PU crystallization process.

3.2.2 Morphology of the PU elastomer and ATT-MDI/PU nanocomposites

The morphology of the ATT–MDI/PU nanocomposites was investigated with TEM and SEM. TEM observations of the ATT–MDI/PU nanocomposite with 2.5 wt % nanorods indicated that the modified ATT nanorods were dispersed quite uniformly in the PU matrix as single crystals or crystal bundles with diameters smaller than 100 nm [Fig. 6(a)]. The relatively good dispersion of nanorods in the PU matrix could be the result of stable hindrance developed between the modified nanorods caused by the grafted MDI chains on the ATT surface; also, the filler increased compatibility with the polymer. Both facts contributed to the dispersion of nanorods and prevented agglomeration. The uniform dispersion illustrates the effectiveness of the two-step modification of ATT for the PU system. However, when the loading of ATT–MDI nanorods was increased to 10 wt %, the dispersion

became less uniform, and agglomeration was observed [Fig. 6(b)]. The agglomeration reduced the effective surface area of ATT–MDI and diminished the interfacial adhesion.

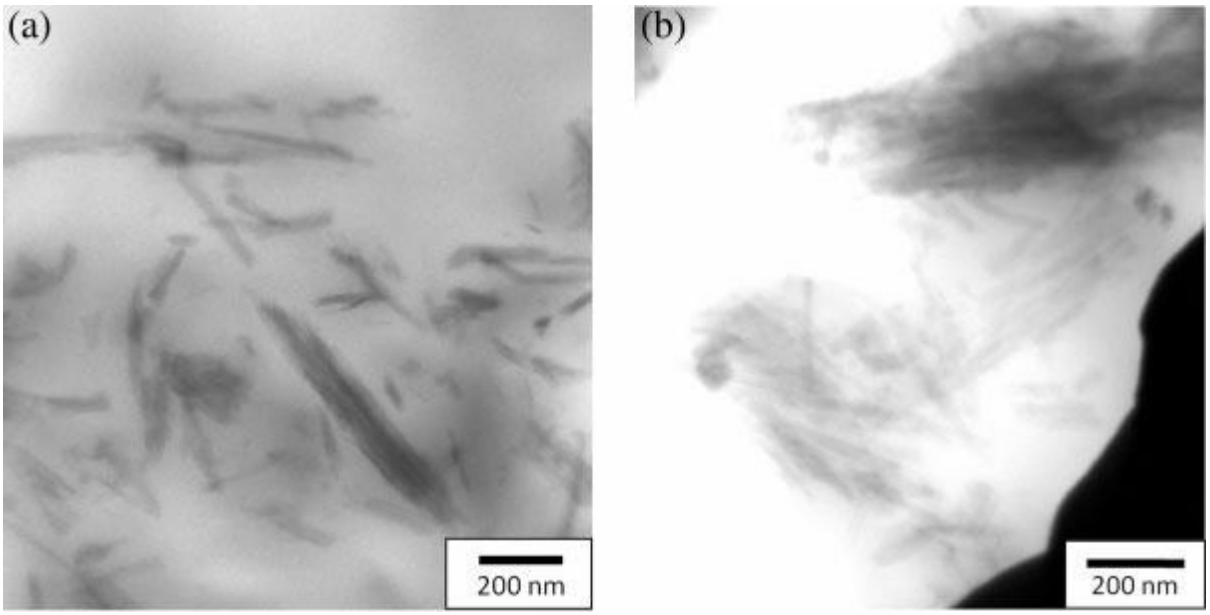

Figure 6: *TEM images of ATT–MDI/PU nanocomposite with (a) 2.5 and (b) 10 wt % nanorods.*

Tensile fracture surfaces of the PU elastomer and the ATT–MDI/PU nanocomposites were examined with SEM. Figure 7 shows typical SEM images of neat PU and ATT–MDI/PU nanocomposites with 5 wt % nanorods. The fracture surface of neat PU [Fig. 7(a)] was uneven but relatively smooth (at 10,000×). In contrast, the fracture surface of the 5 wt % ATT–MDI nanocomposite exhibited pronounced microroughness [Fig. 7(b)]. The microrough morphology evidenced in Figure 7(b) was attributed to the inherent anisotropy and rigidity of ATT–MDI, which caused microscale crack deflection. Because the nanorods were well dispersed in the PU matrix, the interfacial adhesion with the polymeric matrix was enhanced, and the mobility of polymeric molecules in close proximity was restricted [39]. The uneven and rough surface morphology observed for the 5 wt % ATT–MDI/PU

nanocomposite was derived from the presence of ATT and the associated constraints on chain mobility in the PU matrix.

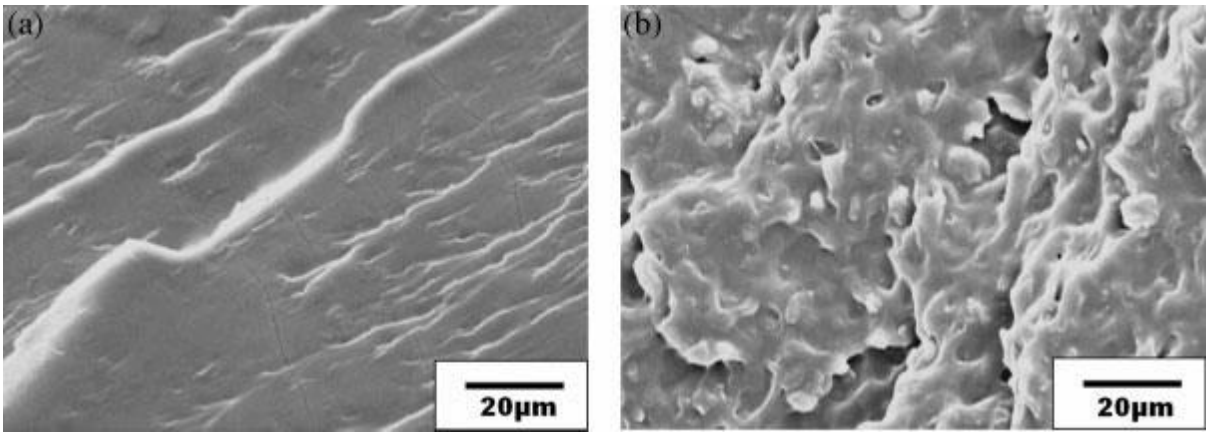

Figure 7: *SEM images of (a) neat PU and (b) the ATT–MDI/PU nanocomposite with 5 wt % nanorods.*

3.2.3 DMA

Table III lists the values of G' at 40 and 100°C as a function of the weight percentage of ATT–MDI as well as the glass-transition temperatures of the hard segment. The G' values at both temperatures (40 and 100°C) increased with increased loadings of ATT–MDI nanorods. An increase in G' of approximately 20% over neat PU was observed for 10 wt % ATT–MDI nanocomposites at 40°C. However, at 100°C, the values of G' for all samples dropped by roughly half, underscoring the heat sensitivity of both neat PU and ATT–MDI/PU nanocomposites within this temperature range. Despite the decrease in G' values at 100°C, the G' values for ATT–MDI/PU nanocomposites still exceeded those of neat PU for most samples. In addition, the G' values for ATT–OH/PU and ATT/PU composites at 40 and 100°C were similar to those of neat PU but less than those of ATT–MDI/PU nanocomposites with the same filler contents. This behavior arose from the chemical

modification of ATT by grafted MDI molecules and the enhanced interfacial adhesion to the PU matrices.

Table 3: *G′ Values at 40 and 100°C and Peaks in Tan δ/Temperature Curves for the Hard Segment*

Sample	***G′* (MPa)**		$T_{g,HS}$ **(°C)**[a]
	40°C	**100°C**	
Neat PU	21.96	10.42	162.6
0.5 wt % ATT–MDI/PU	22.83	9.91	162.8
2.5 wt % ATT–MDI/PU	24.24	12.00	173.8
5 wt % ATT–MDI/PU	24.90	12.48	174.6
10 wt % ATT–MDI/PU	26.18	14.93	189.8
2.5 wt % ATT–OH/PU	23.25	10.82	163.7
2.5 wt % ATT/PU	22.85	10.53	161.3

a Glass-transition temperature of the hard segment.

The glass-transition temperature of the hard segment can be observed from the peaks in the tan δ/temperature curve. An increase in the glass-transition temperature of the hard segment with increasing ATT–MDI loading is evident in the data summarized in Table III. This increase in the glass-transition temperature can be ascribed, at least in part, to the restricted mobility of amorphous polymer chains that results from the physical crosslinks induced by crystallization, as noted by other authors [40, 41]. However, the shift in the glass-transition temperature with increasing additions of ATT–MDI nanorods is so large that it can be explained only as the direct consequence of the decreased flexibility of polymer chains in the presence of stiff crystalline ATT.

Both the ATT–OH/PU and ATT/PU nanocomposites had hard-segment transition temperatures similar to that of neat PU. This observation suggests that the ATT–OH and original ATT did not

substantially restrict the mobility of polymer chains, despite the high filler surface area of these crystalline nanofillers. This was attributed to weak interfacial adhesion in these materials. From the DSC and DMA results, we conclude that the ATT–MDI nanorods, in contrast, induced additional crystallinity within the soft segment but restricted the movement of polymer chains in the hard segment. This behavior was caused by the heterogeneous nanorods, the enhanced interfacial adhesion to the PU matrix, and the coreaction between the filler and polymer.

3.2.4 Tensile Properties

The yield strength and elastic modulus values for different ATT–MDI nanocomposites are plotted as a function of the nanorod filler content in Figure 8. In comparison with neat PU, the tensile properties of the ATT–MDI/PU nanocomposites increased significantly. Figure 8 shows that the Young's modulus and tensile yield strength increased 36 and 12%, respectively, after the addition of 2.5 wt % ATT–MDI nanorods. The 10 wt % ATT–MDI/PU nanocomposite showed increases in the tensile strength and Young's modulus of more than 75% with respect to those of neat PU. The increased modulus arose from the reinforcing effect provided by the ATT–MDI nanorods.

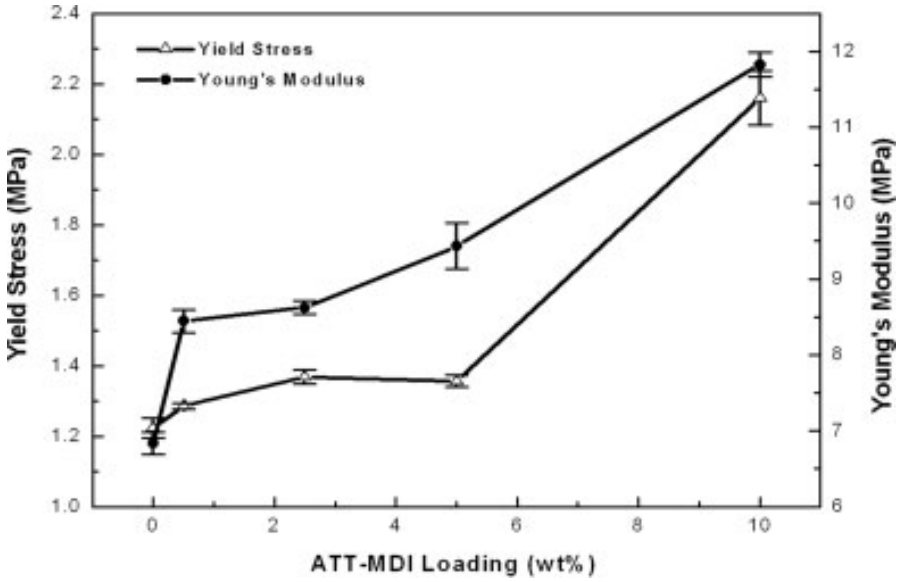

Figure 8: *Yield stress and Young's modulus for the ATT–MDI/PU nanocomposites with different amounts of modified ATT.*

The melting point of the soft segment was close to room temperature. Thus, the tensile properties at room temperature were directly related to the soft-segment characteristics. Korley et al [42] reported that crystallites present within the soft segment might absorb strain energy upon deformation. Thus, semicrystalline soft segments can act as an effective load-bearing phase during deformation [42]. As shown by the DSC measurements, the ATT–MDI rods acted as nucleation seeds, increasing the degree of crystallinity of the soft segment. In addition, the rigid crystalline ATT–MDI nanorods also contributed to the increased hardness by virtue of simple reinforcement.

Nanocomposite specimens containing hydroxyl functional groups on the ATT surface (ATT–OH) and composites prepared from the as-received ATT were also mechanically tested. Unlike the ATT–MDI nanorods, the addition of ATT–OH and ATT nanorods to the polymeric matrix caused decreases in the yield strength and Young's modulus (Fig. 9). As summarized in Table IV, the ATT–MDI/PU nanocomposite exhibited a 40% increase in Young's modulus and a 15–30% increase in the yield strength in comparison with the other composites with similar loadings. These results

illustrate that an adequate dispersion of the rigid filler into the polymer is necessary but not sufficient to enhance composite mechanical properties and that surface or chemical modifications which lead to improved interfacial adhesion between the filler and matrix are also necessary.

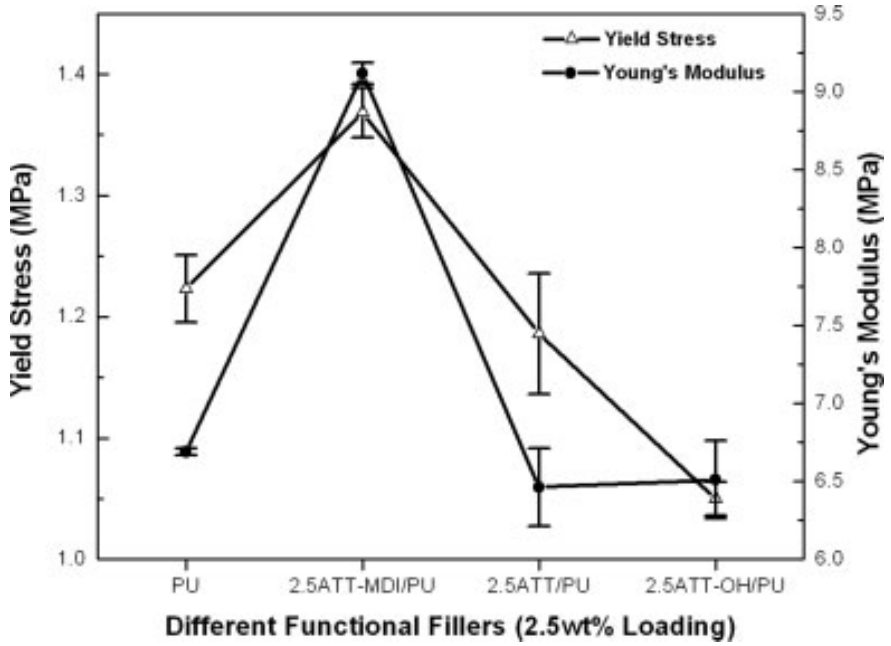

Figure 9: *Yield stress and Young's modulus for different functional fillers of the ATT–MDI/PU composites.*

Table 4: *Young's Modulus and Yield Strength for the ATT/PU Composites with Different Functional Fillers*

Sample	Young's modulus (MPa)	Yield strength (MPa)
Neat PU	6.69	1.22
2.5 wt % ATT–MDI/PU	9.12	1.37
2.5 wt % ATT–OH/PU	6.51	1.05
2.5 wt % ATT/PU	6.46	1.19

3.2.5 Thermal Degradation

Conventional PU is regarded as having poor thermal stability. However, the addition of ATT–MDI nanorods is expected to enhance thermal stability. The decomposition temperature was measured by

TGA for the ATT–MDI/PU nanocomposites and the neat PU, and the results are shown in Figure 10. The profiles of weight loss for PU and ATT–MDI/PU nanocomposites can be divided into two stages (if we ignore the small weight loss below 200°C resulting from adsorbed moisture evaporation). In the first stage (280–370°C), a 25% weight loss occurred, and this was associated with decomposition of the hard segment. The second stage, starting at 370°C for PU and at 380°C for ATT–MDI/PU nanocomposites, involved a major weight loss stemming from soft-segment decomposition, which is consistent with the work of Petrovic et al [43]. Both stages exhibited a difference of at least 10°C in the decomposition temperature when the ATT–MDI/PU nanocomposites were compared with neat PU. This difference arose because the ATT–MDI nanorods acted as a physical barrier in the polymeric network and limited the gas diffusion at the interface, thus affecting the kinetics of the degradation reactions [44].

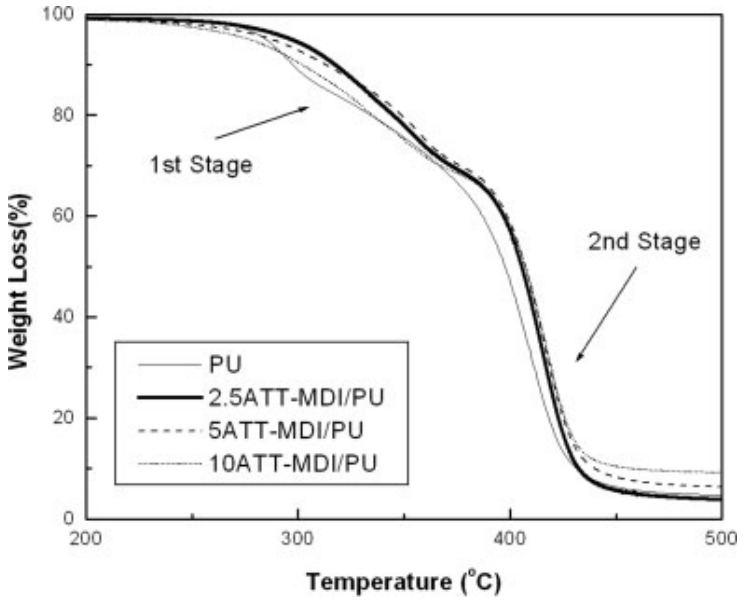

Figure 10: *Thermal degradation behaviors of PU and the ATT–MDI/PU nanocomposites.*

4. Conclusions

ATT/PU nanocomposites were synthesized by a copolymerization reaction after a two-step functionalization of ATT. The resulting nanocomposites exhibited increases in the degree of crystallinity, thermal stability, and mechanical strength in comparison with the neat PU. The findings were attributed to the chemical modification of ATT, which led to suitable surface compatibility and reactivity with the matrix system. A relatively uniform dispersion and strong interfacial adhesion were created by chemical bonding between dispersed and continuous phases. The chemical modification of ATT also facilitated the development of the nanocomposite network. Further improvements and applications in specific polymer matrices are likely possible with optimized surface treatments. The addition of small amounts of nanorods will afford opportunities to design polymers with enhanced properties for adhesives and composite materials.

References:

1. Lin, J. R.; Chen, L. W. J Appl Polym Sci 1998, **69**, 1563.
2. Penczek, P.; Frisch, K. C.; Szczepaniak, B.; Rudnik, E. J Polym Sci Part A: Polym Chem 1993, **31**, 1211.
3. Oertel, G. Polyurethane Handbook; Hanser: Munich, 1985.
4. Bradley, W. F. Am Mineral 1940, **25**, 405.
5. Galan, E. Clay Miner 1996, **31**, 443.
6. Phillips, K. A. Arizona Department of Mines and Mineral Resources; Phoenix, Arizona; 1989, September Report **89-3**.
7. Haydn, M. Mining, Minerals, and Sustainable Development (MMSD) 2002, No. **64**.
8. Li, A.; Wang, A. J Eur Polym 2005, **41**, 1630.
9. Shen, L.; Lin, Y.; Du, Q.; Zhong, W.; Yang, Y. Polymer 2005, **46**, 5758.
10. Kojima, Y.; Usuki, A.; Kawasumi, M.; Okada, A.; Kurauchi, T.; Kamigaito, O. J Polym Sci Part A: Polym Chem 1993, **31**, 983.
11. Kojima, Y.; Usuki, A.; Kawasumi, M.; Okada, A.; Kurauchi, T.; Kamigaito, O.; Kaji, K. J Polym Sci Part B: Polym Phys 1994, **32**, 625.
12. Kojima, Y.; Usuki, A.; Kawasumi, M.; Okada, A.; Kurauchi, T.; Kamigaito, O.; Kaji, K. J Polym Sci Part B: Polym Phys 1995, **33**, 1039.
13. Ni, P.; Li, J.; Suo, J.; Li, S. J Mater Sci 2004, **39**, 4671.
14. Wang, M. J. Rubber Chem Technol 1998, **71**, 520.

Please cite this article as: C-H Wang, M.L. Auad, N.E. Marcovich, and S. Nutt. **Synthesis and characterization of organically modified attapulgite/polyurethane nanocomposites**, J App Polymer Sci 109 [4] (2008) 2562-2570. DOI:http://dx.doi.org/doi:10.1002/app.28254

15. Boonstra, B. B. In Rubber Technology and Manufacture, 2nd ed.; Blow, C. M.; Hepbum, C., Eds.; Butterworth: London, 1982; Chapter 7.
16. Bicerano, J.; Brewbaker, J. L. J Chem Soc Faraday Trans 1995, **91**, 2507.
17. Calvert, P. Nature 1999, **399**, 210.
18. Shaffer, M. S. P.; Windle, A. H. Adv Mater 1999, **11**, 937.
19. Xia, H.; Wang, Q.; Qiu, G. Chem Mater 2003, **15**, 3879.
20. Kashiwagi, T.; Grulke, E.; Hilding, J.; Awad, R.; Harris, W.; Douglas, J. Macromol Rapid Commun 2002, **23**, 761.
21. Qin, S. H.; Qin, D. Q.; Ford, W. T.; Resasco, D. E.; Herrera, J. E. J Am Chem Soc 2004, **126**, 170.
22. Andrews, R.; Jacques, D.; Minot, M.; Rantell, T. Macromol Mater Eng 2002, **7**, 395.
23. Xia, H.; Song, M. Soft Matter 2005, **1**, 386.
24. Purcell, R. J., Jr.; Parker, D. C. U.S. Pat. 6,444,601 (2002).
25. Guo, Z.-X.; Liu, W.-F.; Li, Y.; Yu, J. J Macromol Sci Chem 2005, **42**, 221.
26. Prisacariu, C.; Olley, R. H.; Caraculacu, A. A.; Bassett, D. C.; Martin, C. Polymer 2003, **44**, 5407.
27. Chen-Yang, Y. W.; Lee, Y. K.; Chen, Y. T.; Wu, J. C. Polymer 2007, **48**, 2969.
28. Myriam, M.; Suarez, M.; Martin Pozas, J. M. Clays Clay Minerals 1998, **46**, 225.
29. Fripiat, J. J.; Leonard, A.; Barake, N. Bull Soc Chim 1963, **1**, 122.
30. Pattanayak, A.; Jana, S. C. Polymer 2005, **46**, 5183.
31. Kuptsov, A. H.; Zhizhin, G. N. Handbook of Fourier Transform Raman and Spectra of Polymers; Elsevier: New York, 1988.
32. Chattopadhyay, D. K.; Raju, K. V. S. N. Polym Sci 2007, **32**, 352.
33. Speckhard, T. A.; Hwang, K. K. S.; Yang, C. Z.; Laupan, W. R.; Cooper, S. L. J Macromol Sci Phys 1984, **23**, 175.
34. MacKnight, W. J.; Yang, M.; Kajiyama, T. Polym Prepr (Am Chem Soc Div Polym Chem) 1968, **9**, 860.
35. Yang, C. Z.; Hwang, K. K. S.; Cooper, S. L. Makromol Chem 1983, **184**, 651.
36. Yilgor, I.; Riffle, J. S.; Wilkes, G. L.; McGrath, J. E. Polym Bull (Berlin) 1982, **8**, 535.
37. Li, Y.; Tong, G.; Liu, J.; Linliu, K.; Desper, C. R.; Chu, B. Macromolecules 1992, **25**, 7365.
38. Sun, L.; Yang, J.-T.; Lin, G.-Y.; Zhong, M.-Q. Mater Lett 2007, **61**, 3963.
39. Etan, A.; Fisher, F. T.; Andrews, R.; Brinson, L. C.; Schadler, L. S. Compos Sci Technol 2006, **66**, 1159.
40. Mathew, A. P.; Dufresne, A. Biomacromolecules 2002, **3**, 609.
41. Auad, M. L.; Contos, V. S.; Nutt, S.; Aranguren, M. I.; Marcovich, N. E. Polym Int 2007, **67**, 651.
42. Korley, J.; LaShanda, T.; Pate, B. D.; Thomas, E. L.; Hammond, P. T. Polymer 2006, **47**, 3073.
43. Petrovic, Z. S.; Zavargo, Z.; Flynn, J. H.; MacKnight, W. J. J Appl Polym Sci 1994, **51**, 1087.
44. Golebiewski, J.; Galeski, A. Compos Sci Technol 2007, **67**, 3442.

Please cite this article as: C-H Wang, M.L. Auad, N.E. Marcovich, and S. Nutt. **Synthesis and characterization of organically modified attapulgite/polyurethane nanocomposites**, J App Polymer Sci 109 [4] (2008) 2562-2570. DOI:http://dx.doi.org/doi:10.1002/app.28254